Supporting Information

Diamine-functionalized metal-organic framework: Exceptionally high CO_2 capacities from ambient air and flue gas, ultrafast CO_2 uptake rate, and adsorption mechanism

Woo Ram Lee, Sang Yeon Hwang, Dae Won Ryu, Kwang Soo Lim, Sang Soo Han, Dohyun Moon, Jungkyu Choi, and Chang Seop Hong*

Powder X-ray Diffraction and Structure Modeling. PXRD data were recorded using Cu Kα (λ = 1.5406 Å) on a Rigaku Ultima III diffractometer with a scan speed of 2°/min and a step size of 0.01°. The synchrotron powder X-ray diffraction data were collected at 298K with the 240 mm of detector distance in 2400 s exposure with synchrotron radiation (λ = 1.09998Å) using a 2D SMC ADSC Quantum-210 detector with a silicon (111) double crystal monochromator at the Pohang Accelerator Laboratory. The ADX program[1] was used for data collection, and Fit2D program[2] was used for converting a two-dimensional diffraction image to a one-dimensional diffraction pattern. The unit cell dimensions of **1-DMF**, **1**, **1-en**, and **1-en-CO_2** were determined by conducting a full-pattern decomposition with the Le Bail method (Pawley refinement) implemented in *TOPAS-Academic*. The trigonal space group $P3_221$ was utilized for the refinements, due to the isomorphism with Zn_2(dobpdc).[3] Based on the unit cell dimensions obtained, the geometry of the backbones was optimized via an energy minimization algorithm using the universal force field implemented in the *Forcite* module of *Materials Studio*.[4]

Gas Sorption Measurements. Gas sorption isotherms were measured using a Micromeritics ASAP2020 instrument up to 1 atm of gas pressure unless otherwise stated. The highly pure N_2 (99.999%), CO_2 (99.999%), and O_2 (99.995%) were used in the sorption experiments. N_2 gas isotherms were measured at 77 K and 298 K, and O_2 isotherm was collected at 298 K, and CO_2 uptake was measured at 298 K, 323 K, 348 K, 373 K, 393 K, and 423 K.

Thermogravimetric Analyses and Gas Cycling Measurements. Thermogravimetric analyses (TGA) were carried out at a ramp rate of 2 °C/min in an Ar (99.999 %) flow using a Scinco TGA N-1000 instrument. CO_2 cycling experiments of the activated **1** were carried out on the instrument with 15% CO_2 in N_2, 390 ppm CO_2 in air (390 ppm CO_2 and 21% O_2 balanced with N_2), and Ar (99.999 %). A flow rate of 60 mL/min was applied for all gases. We conducted cycling experiments using a fresh sample [Mg_2(dobpdc)$(en)_{1.7}(H_2O)_{0.3}$] (**1-en**), in which more en was grafted onto the open metal sites, to check the N/Mg ratio. Elemental analyses indicate that the N/Mg ratio was maintained before (N/Mg = 1.7) and after the TSA cycles (N/Mg = 1.7) and no amine loss was observed.

Infrared Spectroscopy Measurements. Infrared spectra were obtained with KBr pellets and an air-tight homemade IR cell composed of NaCl windows using a Bomen MB-104 spectrometer. Prior to the IR measurements, N_2 was purged into a sample chamber, a detector, and an IR source to remove CO_2 in air. Variable temperature infrared spectra were collected with a homemade IR cell sandwiched by two CaF_2 windows using a Varian 640-IR spectrometer. For this experiment, N_2 was purged into a sample chamber.

Other Physical Measurement. Elemental analyses for C, H, and N were performed at the Elemental Analysis Service Center of Sogang University.

[Reference]

1. A. J. Arvai, C. Nielsen, ADSC Quantum-210 ADX Program, Area Detector System Corporation; Poway, CA, USA, 1983.
2. Fit2D Program: Hammersley, A. (E-mail: hammersley@esrf.fr), ESRF, 6 RUE JULES HOROWITZ BP 220 38043 GRENOBLE CEDEX 9 FRANCE.
3. T. M. McDonald, W. R. Lee, J. A. Mason, B. M. Wiers, C. S. Hong, J. R. Long, *J. Am. Chem. Soc.* **2012**, *134*, 7056-7065.
4. H. Deng, S. Grunder, K. E. Cordova, C. Valente, H. Furukawa, M. Hmadeh, F. Gandara, A. C. Whalley, Z. Liu, S. Asahina, H. Kazumori, M. O'Keeffe, O. Terasaki, J. F. Stoddart, O. M. Yaghi, *Science* **2012**, *336*, 1018-1023.

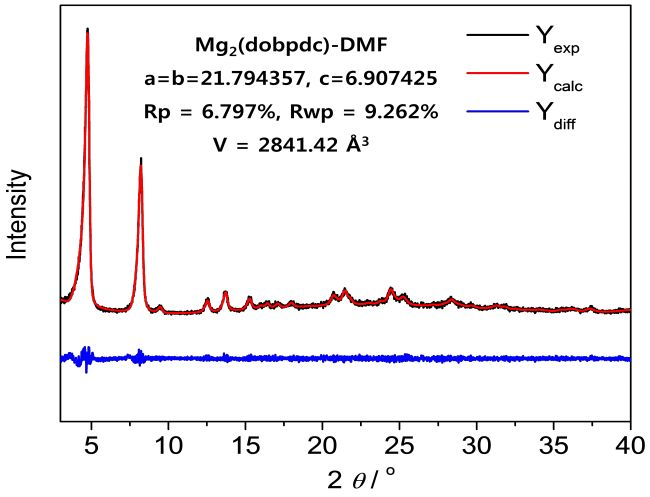

Fig. S1. Powder X-ray diffraction pattern of **1-DMF** (black) with calculated diffraction pattern (red) from Pawley refinement with difference (blue).

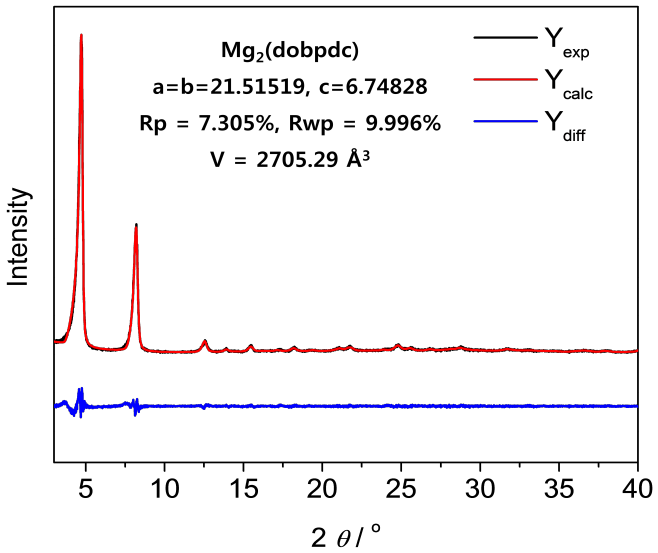

Fig. S2. Powder X-ray diffraction pattern of the activated **1** (black) with calculated diffraction pattern (red) from Pawley refinement with difference (blue).

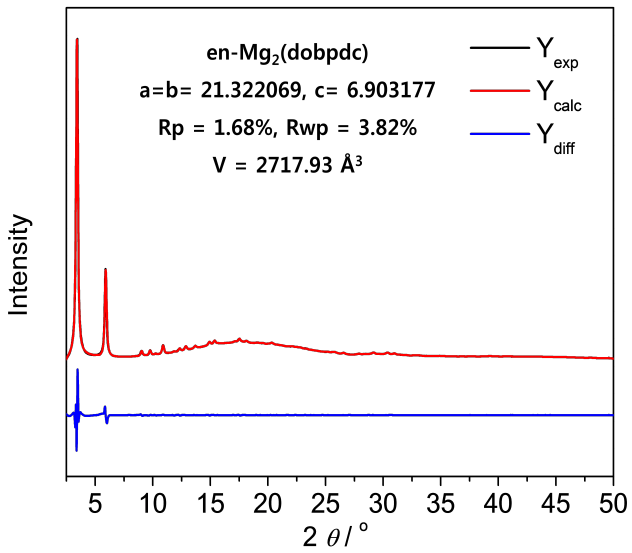

Fig. S3. Synchrotron powder X-ray diffraction pattern of **1-en** (black) with calculated diffraction pattern (red) from Pawley refinement with difference (blue).

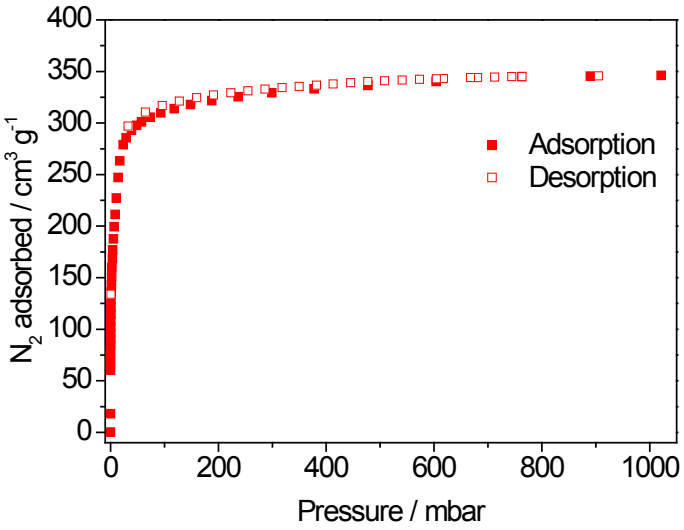

Fig. S4. N_2 adsorption isotherm in **1-en** at 77 K.

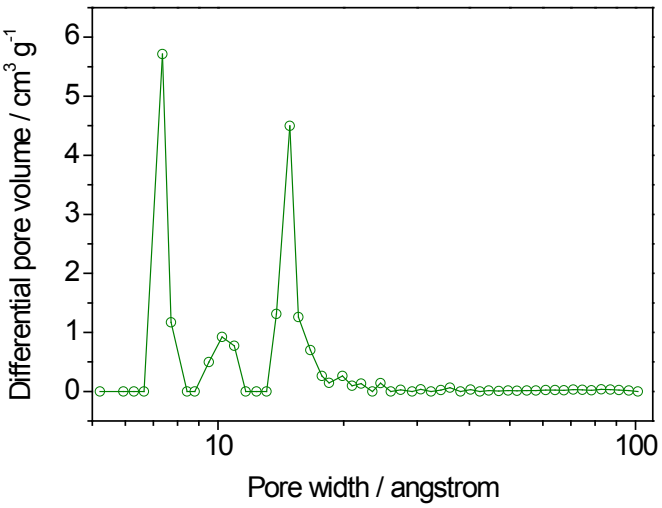

Fig. S5. DFT pore size distribution for **1-en** calculated from N_2 adsorption at 77 K using a Tarazona NLDFT with a cylinder pore geometry.

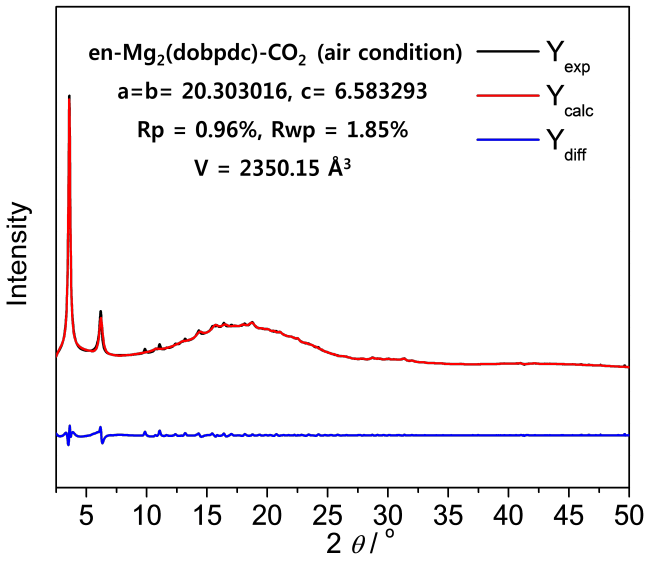

Fig. S6. Synchrotron powder X-ray diffraction pattern of **1-en-CO_2** (adsorbed at ambient air condition) (black) with calculated diffraction pattern (red) from Pawley refinement with difference (blue).

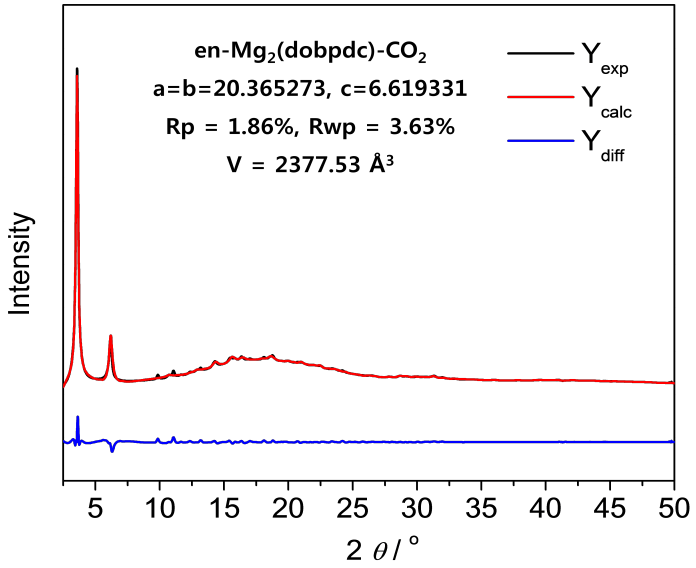

Fig. S7. Synchrotron powder X-ray diffraction pattern of **1-en-CO_2** (black) with calculated diffraction pattern (red) from Pawley refinement with difference (blue).

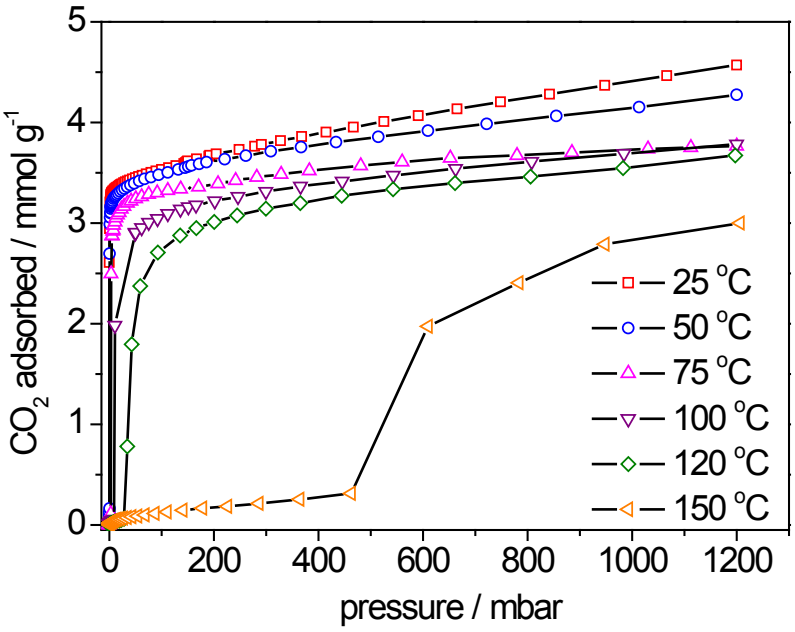

Fig. S8. CO_2 adsorption isotherms for **1-en** at 25 °C, 50 °C, 75 °C, 100 °C, 120 °C and 150 °C.

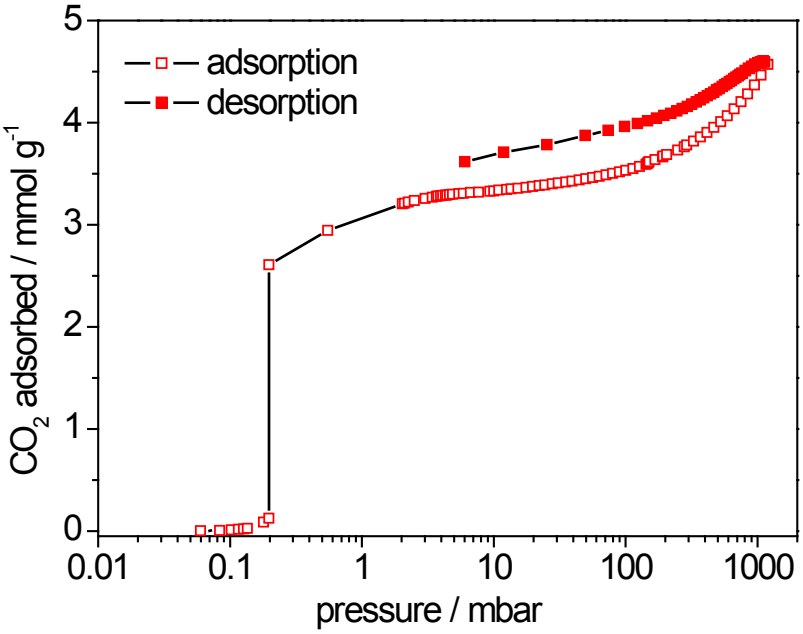

Fig. S9. Experimental isotherms of CO_2 adsorption (empty shapes) and desorption (filled shapes) for **1-en** at 25 °C.

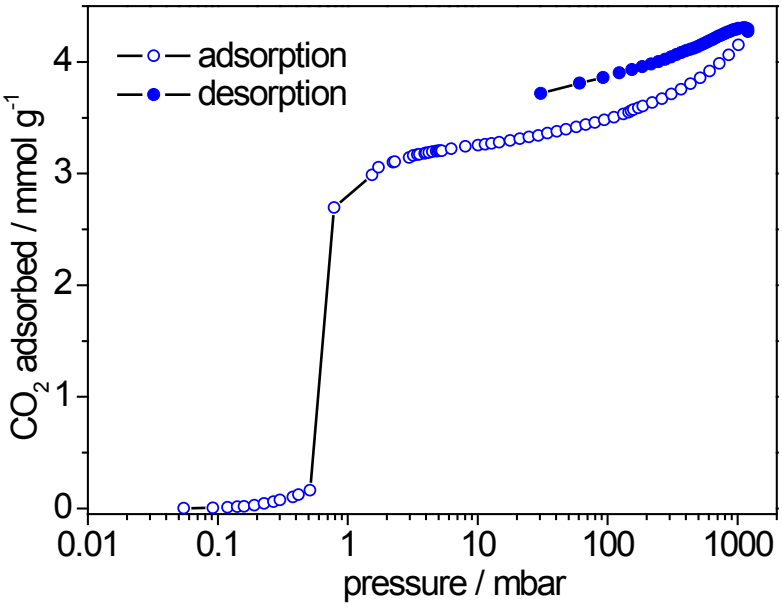

Fig. S10. Experimental isotherms of CO_2 adsorption (empty shapes) and desorption (filled shapes) for **1-en** at 50 °C.

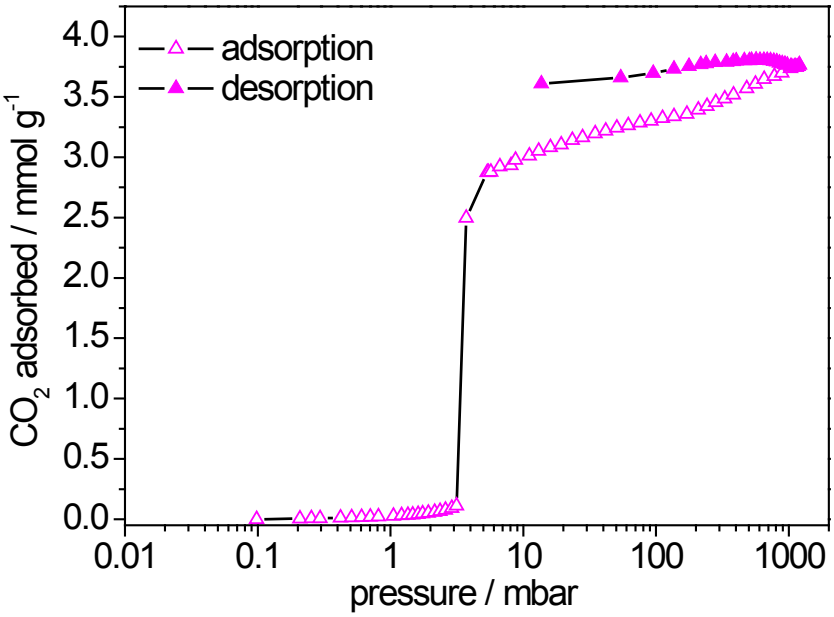

Fig. S11. Experimental isotherms of CO_2 adsorption (empty shapes) and desorption (filled shapes) for **1-en** at 75 ^{o}C.

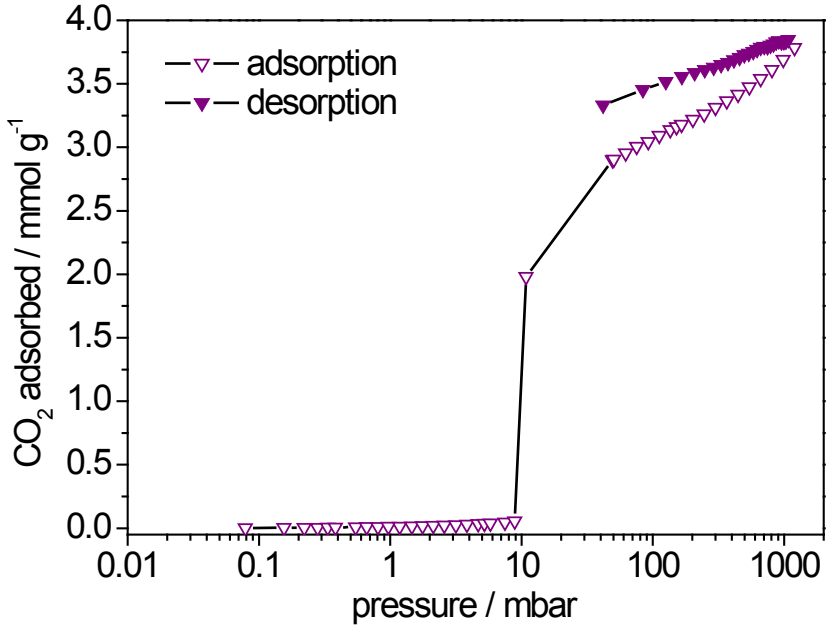

Fig. S12. Experimental isotherms of CO_2 adsorption (empty shapes) and desorption (filled shapes) for **1-en** at 100 ^{o}C.

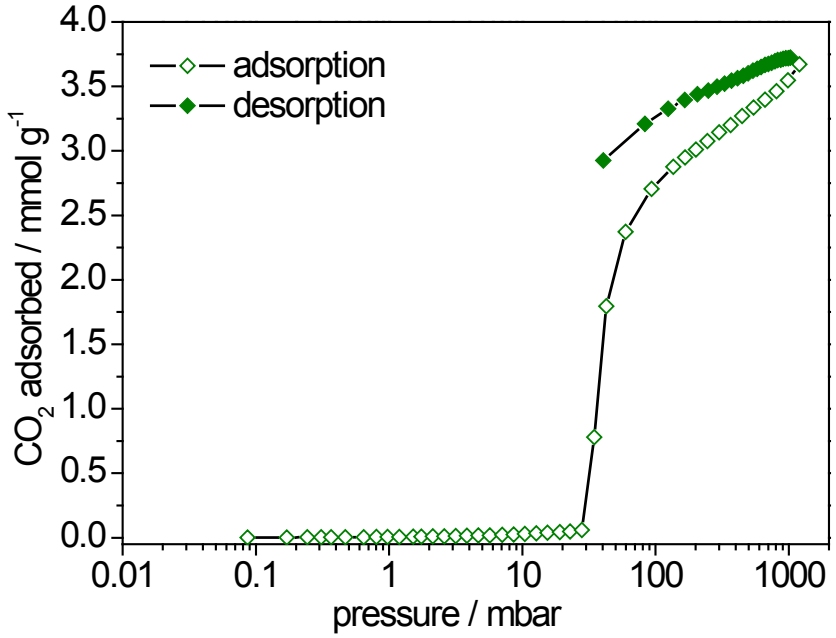

Fig. S13. Experimental isotherms of CO_2 adsorption (empty shapes) and desorption (filled shapes) for **1-en** at 120 °C.

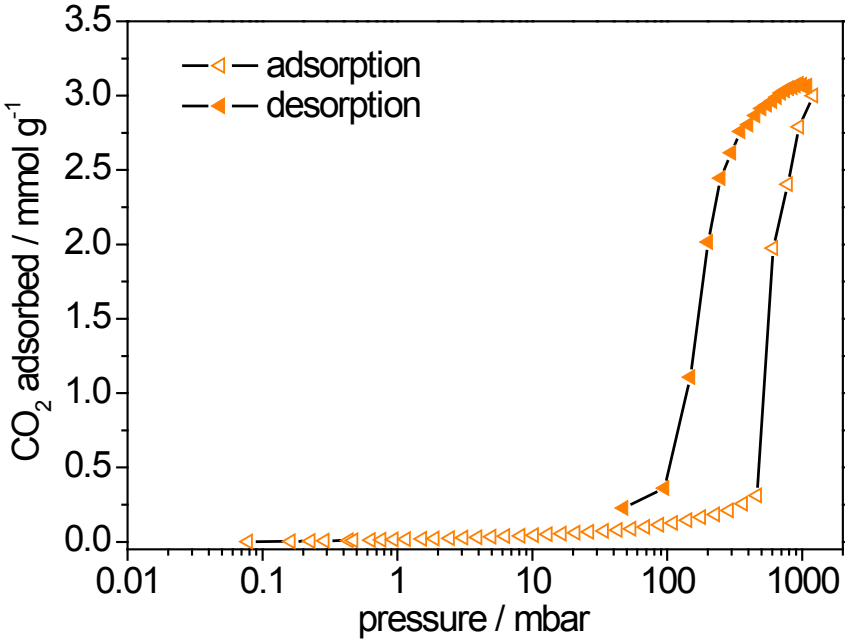

Fig. S14. Experimental isotherms of CO_2 adsorption (empty shapes) and desorption (filled shapes) for **1-en** at 150 °C.

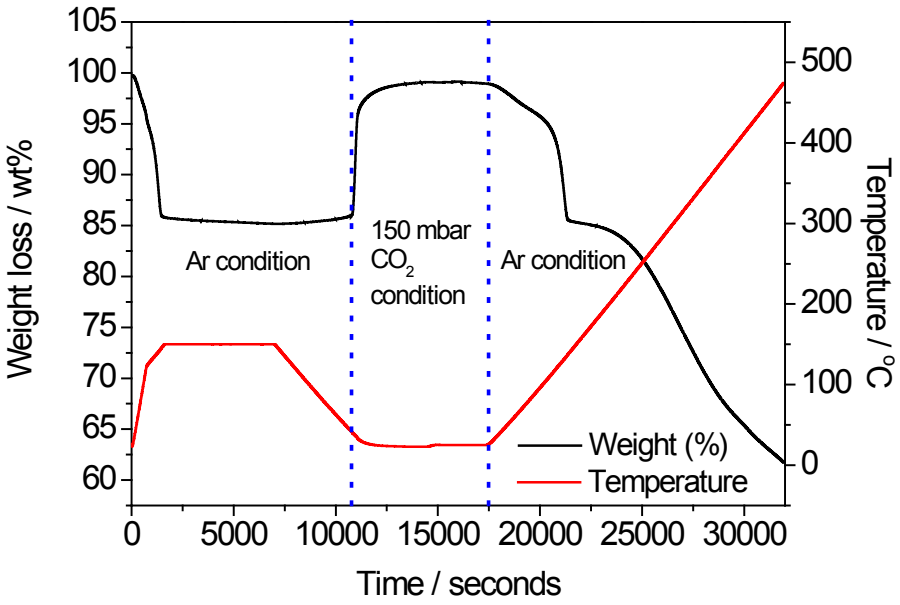

(a)

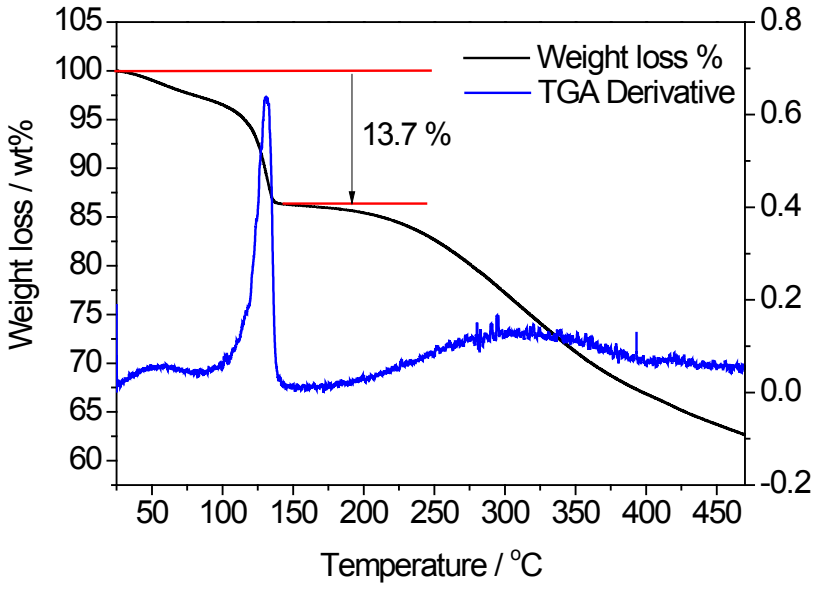

(b)

Fig. S15. TGA curve of **1-en** as a function of a) time, and b) temperature after 290 min.

Table S1. Dual-Site Langmuir-Freundlich parameters for the pre-step region of the CO_2 adsorption isotherm for **1-en** at 25 ^{o}C and 75 ^{o}C.

	25 ^{o}C	**75 ^{o}C**
$q_{sat,\,A}$ / mmol g^{-1}	2.05	0.93
b_A / bar^{-a}	92.02	3.5×10^{-2}
α_A	4.48	1.20
$q_{sat,\,B}$ / mmol g^{-1}	6.2×10^{-2}	2.77
b_B / bar^{-a}	4.9×10^{-2}	4.4×10^{-13}
α_B	8.8×10^{-16}	19.33

Table S2. Modified dual-Site Langmuir-Freundlich parameters for the post-step region of the CO_2 adsorption isotherm for **1-en** at 25 ^{o}C and 75 ^{o}C.

	25 ^{o}C	**75 ^{o}C**
P_{step}	0.20	3.43
$q_{sat,\,A}$ / mmol g^{-1}	2.59	1.10
b_A / bar^{-a}	1.1×10^{44}	3.61
α_A	4.85	2.7×10^{-15}
$q_{sat,\,B}$ / mmol $^{g-1}$	0.76	1.14
b_B / bar^{-a}	2.4	10.39
α_B	0.74	0.97
$q_{sat,\,C}$ / mmol $^{g-1}$	6.5×10^{-3}	0.85
b_C / bar^{-a}	1.5×10^{45}	1.9×10^{44}
α_C	1.47	1.07

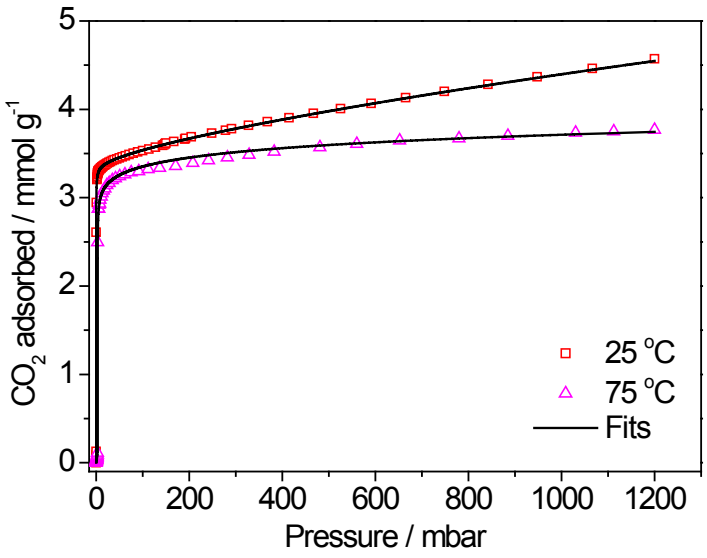

Fig. S16. CO_2 isotherms and fits based on a dual-site Langmuir-Freundlich equation for **1-en** at 25 °C and 75 °C.

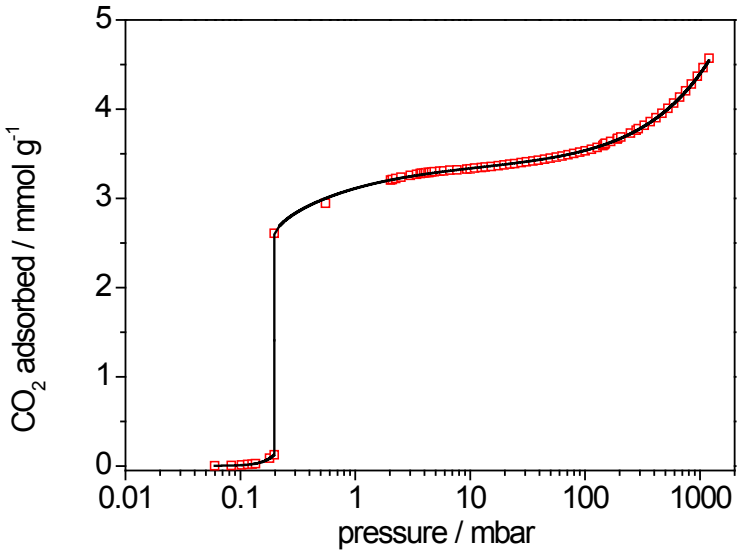

Fig. S17. CO_2 isotherm and a fit based on a dual-site Langmuir-Freundlich equation for **1-en** at 25 °C plotted on a logarithmic scale.

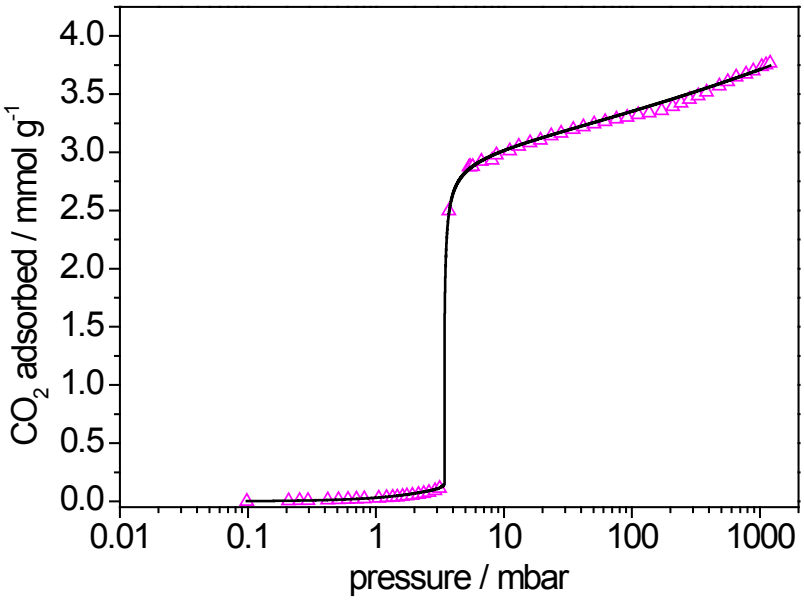

Fig. S18. CO_2 isotherm and a fit based on a dual-site Langmuir-Freundlich equation for **1-en** at 75 °C plotted on a logarithmic scale.

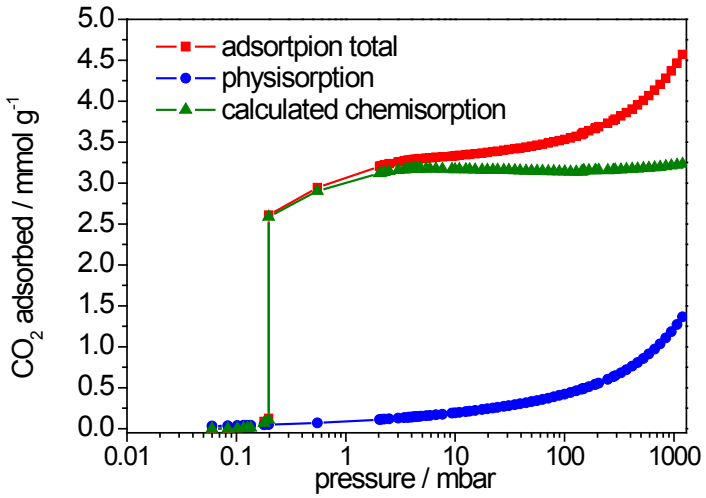

Fig. S19. CO_2 isotherm (red) at 25 °C including chemisorption and physisorption. After saturation, the sample was evacuated for 4 h to remove all physisorbed CO_2. We recorded again the CO_2 adsorption data that only show a physisorptive contribution (blue). The chemisorption contribution (green) was estimated by the subtraction of adsorption total from physisorption part.

We calculated the binding energies of CO_2 with **1-en** using density functional theory (DFT) with van der Waals correction (called the DFT-*ulg*[1] method) in the VASP[2] program. The three-dimensional structures of **1-en** were optimized in rhombo hedral crystal structure (primitive cell) using the Perdew-Burke-Ernzerhof (PBE)[3] exchange-correlation functional. Valence electrons were described by a plane wave basis set with an energy cutoff of 520 eV. And, due to the large size of the cell (156 atoms), the calculations were performed at the gamma (Γ) point.

[References]

1. H. Kim, J.-M. Choi, W. A. III. Goddard, *J. Phys. Chem. Lett.* **2012**, *3*, 360.
2. G. Sun, J. Kürti, P. Rajczy, M. Kertesz, J. Hafner, G. Kresse, *J. Mol. Struct. (THEOCHEM)* **2003**, *624*, 37.
3. J. P. Perdew, K. Burke, M. Ernzerhof, *Phys. Rev. Lett.* **1996**, *77*, 3865.

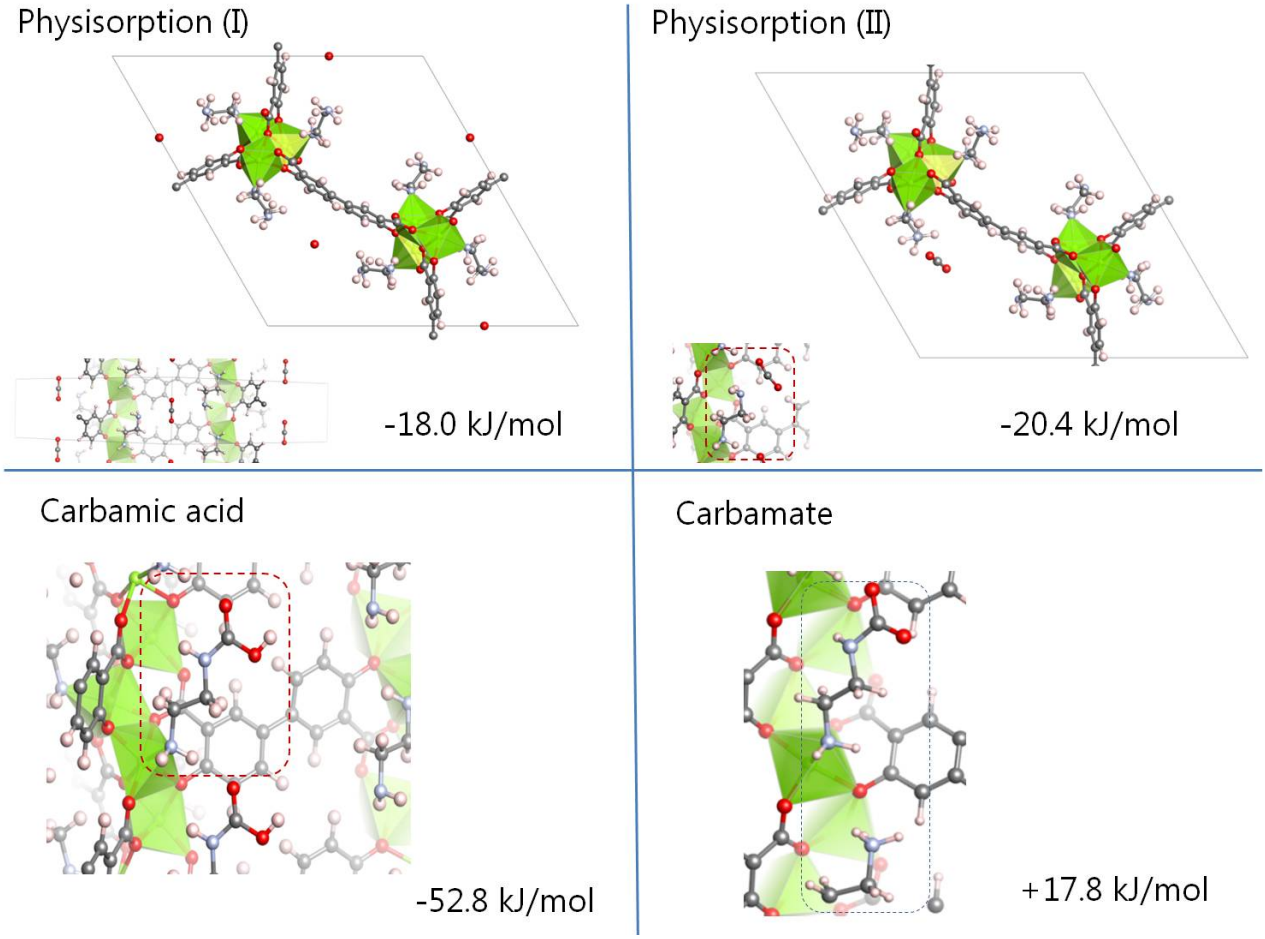

Fig. S20. DFT calculations of the binding energies for the CO_2 adsorption onto **1-en**.

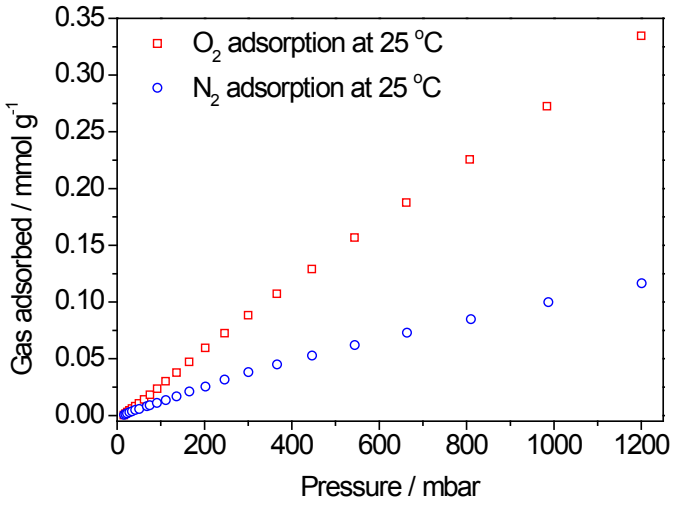

Fig. S21. O_2 (red squares) and N_2 (blue circles) isotherms for **1-en** at 25 °C. The data were obtained by ASAP2020 instrument.

Table S3. The CO_2 selectivity of **1-en** at 25 °C

mixture	other gas	pressure / mbar		uptake / mmol g^{-1}		selectivity	purity / %
		CO_2	other gas	CO_2	other gas		
air	N_2	0.4	800	2.92	0.084	70 000	97
air	O_2	0.4	200	2.92	0.056	26 000	98
flue gas	N_2	150	750	3.62	0.080	230	98

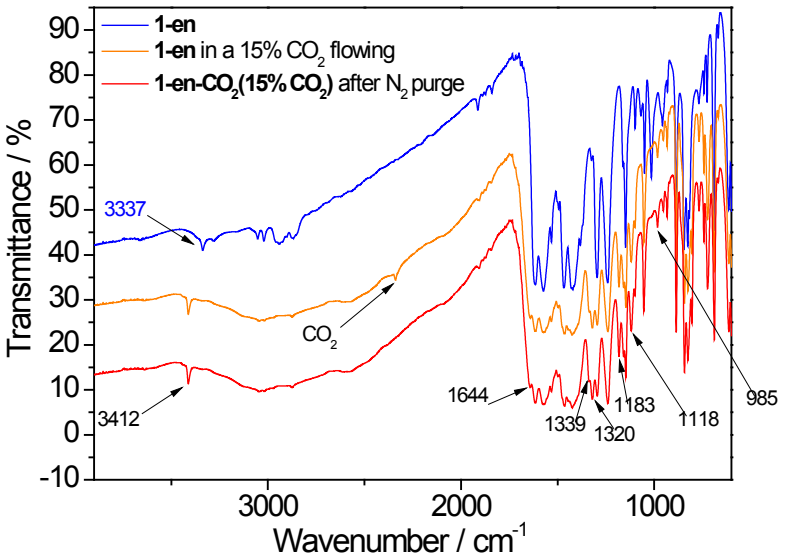

Fig. S22. In-situ IR data of **1-en**, and **1-en** in a 15% CO_2 flowing that corresponds to **1-en-CO_2(15% CO_2)**. The IR spectrum of **1-en-CO_2** after N_2 purge was obtained by a N_2 flowing over **1-en-CO_2(15% CO_2)** for 1 min. We used an air-tight IR cell (NaCl windows) and an oil bubbler to isolate the cell atmosphere from air.

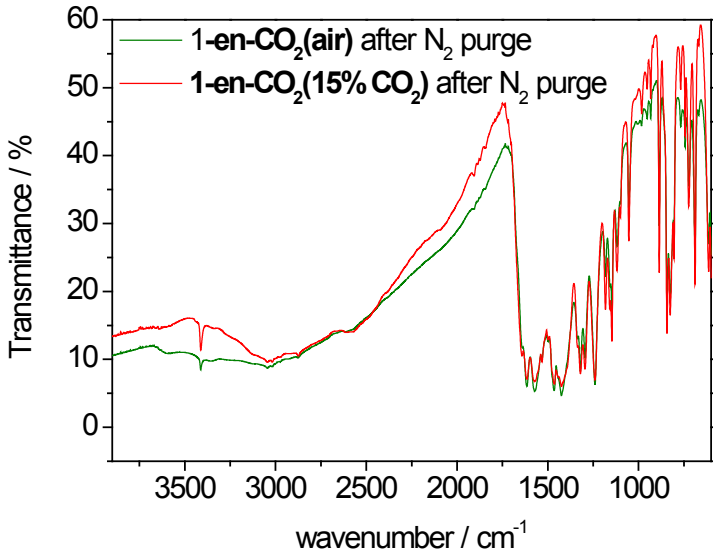

Fig. S23. FT-IR data of **1-en-CO_2(air)** that was obtained by exposing **1-en** to the ambient air and purging with N_2. The IR data for **1-en-CO_2(air)** and **1-en-CO_2(15% CO_2)** are identical from each other. We used an air-tight IR cell (NaCl windows) and an oil bubbler to isolate the cell atmosphere from air.

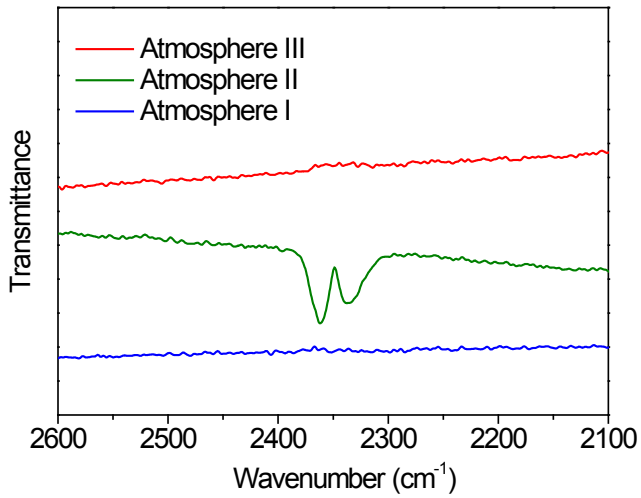

Fig. S24. In-situ FT-IR data of the atmospheres inside the IR cell. Atmosphere I stands for the IR signal in the CO_2 stretching region only under N_2 flowing. Atmosphere II denotes the IR signal of the atmosphere inside the IR cell containing **1-en** into which the simulated air (390 ppm CO_2 and 21% O_2 balanced with N_2) was flowing. Atmosphere III was taken after 2 min of Atmosphere II. We used an air-tight IR cell (NaCl windows) and an oil bubbler to isolate the cell atmosphere from air.

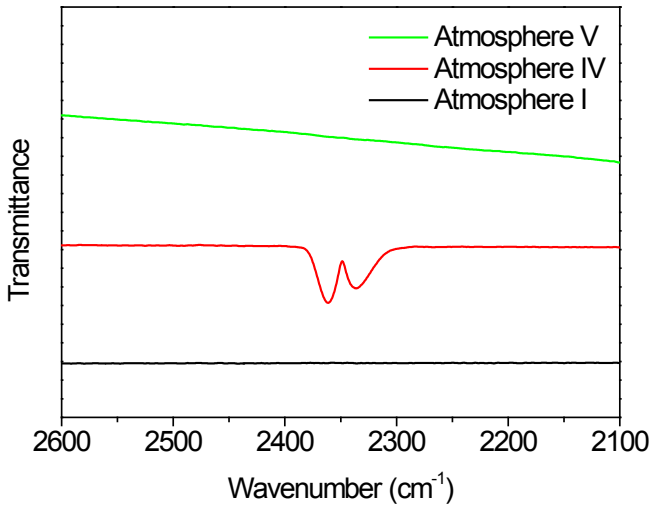

Fig. S25. In-situ FT-IR data of the atmospheres inside the IR cell. Atmosphere I is the same as that in Fig. S25. Atmosphere IV denotes the IR signal of the atmosphere inside the IR cell containing **1-en** into which the ambient air was flowing using a syringe. Atmosphere V was taken after 4 min of Atmosphere IV. We used an air-tight IR cell (NaCl windows) and an oil bubbler to isolate the cell atmosphere from air.

Table S4. Estimated rate of inital adsorption for porous solids.

Materials	Rate (wt %/s)
1-en	0.37
mmen-Mg_2(dobpdc)	0.23
1	0.21
Mg-MOF-74	0.13
Zeolite 13X	0.07
MOF-5	0.00

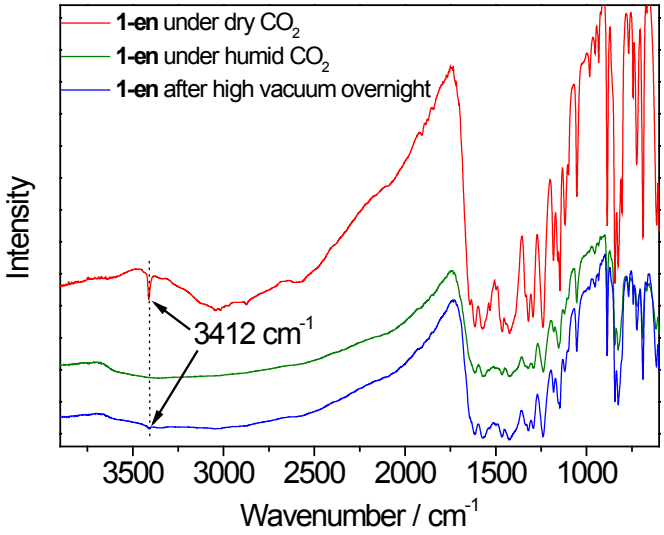

Fig. S26. In-situ IR data of **1-en** under dry CO_2, **1-en** in 100% RH CO_2, and **1-en** after **1-en**-under-humid-CO_2 was treated in high vacuum overnight. The cell and IR instrument were purged with N_2 to remove CO_2 prior to the IR measurements. We used an air-tight IR cell (NaCl windows) and an oil bubbler to isolate the cell atmosphere from air.

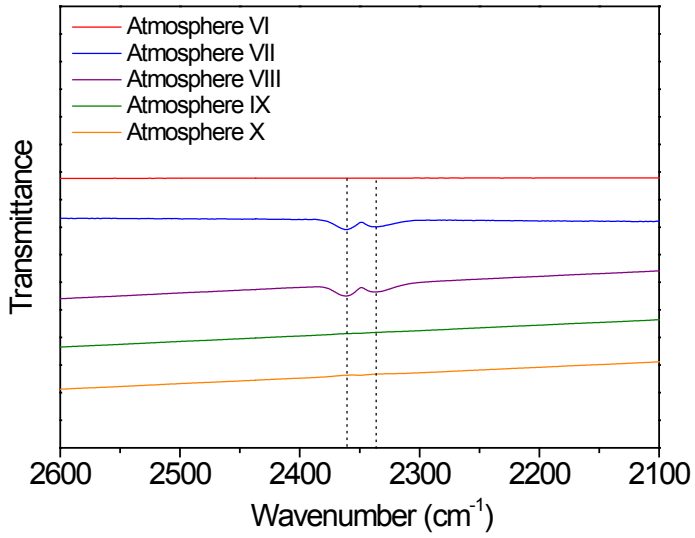

Fig. S27. In-situ FT-IR data of the atmospheres inside the IR cell. Atmosphere VI stands for the IR signal in the CO_2 stretching region only under Ar flowing and Atmosphere VII is under a flowing of humid air. The IR signal of the atmosphere inside the IR cell containing **1-en** was taken after 3 min of Atmosphere VII (Atmosphere VIII), after 4 min (Atmosphere IX), and after 5 min (Atmosphere X). We used an air-tight IR cell (NaCl windows) and an oil bubbler to isolate the cell atmosphere from air.